Atmos. Meas. Tech. Discuss., 7, 10585–10617, 2014
www.atmos-meas-tech-discuss.net/7/10585/2014/
doi:10.5194/amtd-7-10585-2014

Atmospheric Measurement Techniques Discussions
Open Access

Characterization and first results of an ice nucleating particle measurement system based on counterflow virtual impactor technique

L. P. Schenk[1], S. Mertes[1], U. Kästner[1], F. Frank[2], B. Nillius[2,*], U. Bundke[2,], D. Rose[2], S. Schmidt[3], J. Schneider[3], A. Worringen[4], K. Kandler[4], N. Bukowiecki[5], M. Ebert[4], J. Curtius[2], and F. Stratmann[1]**

[1]Leibniz Institute for Tropospheric Research, Leipzig, Germany
[2]Institute for Atmospheric and Environmental Sciences, Goethe University of Frankfurt am Main, Frankfurt am Main, Germany
[3]Max Planck Institute for Chemistry, Particle Chemistry Department, Mainz, Germany
[4]Technical University of Darmstadt, Institute of Applied Geosciences, Darmstadt, Germany
[5]Laboratory of Atmospheric Chemistry, Paul Scherrer Institute (PSI), Villigen, Switzerland
[*]now at: Max Planck Institute for Chemistry, Particle Chemistry Department, Mainz, Germany
[**]now at: Julich Research Center, Institute of Energy and Climate Research, Troposphere (IEK-8), Jülich, Germany

Received: 11 September 2014 – Accepted: 26 September 2014 – Published: 21 October 2014

Correspondence to: L. P. Schenk (schenk@tropos.de)

Published by Copernicus Publications on behalf of the European Geosciences Union.

AMTD

7, 10585–10617, 2014

Sampling of ambient ice nucleating particles

L. P. Schenk et al.

Abstract

A specific instrument combination was developed to achieve a better microphysical and chemical characterization of atmospheric aerosol particles that have the potential to act as ice nucleating particles (INP). For this purpose a pumped counterflow virtual impactor system called IN-PCVI was set up and characterized to separate ice particles that had been activated on INP in the Fast Ice Nucleus Chamber (FINCH) from interstitial, non-activated particles. This coupled setup consisting of FINCH (ice particle activation and counting), IN-PCVI (INP separation and preparation), and further aerosol instrumentation (INP characterization) had been developed for the application in field experiments. The separated INP were characterized on-line with regard to their total number concentration, number size distribution and chemical composition, especially with the Aircraft-based Laser Ablation Aerosol Mass Spectrometer ALABAMA. Moreover, impactor samples for electron microscopy were taken. Due to the coupling the IN-PCVI had to be operated with different flow settings than known from literature, which required a further characterization of its cut-off-behavior. Taking the changed cut-off-behavior into account, the INP number concentration measured by the IN-PCVI system was in good agreement with the one detected by the FINCH optics for water saturation ratios up to 1.01 (ice saturation ratios between 1.21–1.34 and temperatures between −18 and −26 °C). First field results of INP properties are presented which were gained during the INUIT-JFJ/CLACE 2013 campaign at the high altitude research station Jungfraujoch in the Bernese Alps, Switzerland (3580 m a.s.l.).

1 Introduction

Ice crystals in clouds influence precipitation and the microphysical and thus the radiative properties of clouds. They play an important role for the cloud lifetime, the interactions of clouds with solar radiation, cloud electricity and cloud dynamics. Mixed-phase clouds consisting of supercooled droplets and ice particles exist at altitudes where temperatures warmer than −38 °C occur. In such clouds, ice can only be formed heterogeneously, due to the presence of so-called ice nucleating particles (INP) (Vali et al., 2014; DeMott et al., 2011; Pruppacher and Klett, 1997). Known pathways of heterogeneous ice formation are deposition nucleation and condensation, immersion and contact freezing. Field data and modeling studies indicate for many situations that liquid water droplets are a prerequisite for ice formation (Murray et al., 2012; Westbrook and Illingworth, 2011; de Boer et al., 2011; Ansmann et al., 2009). This suggests an important role of immersion and contact freezing processes in atmospheric ice formation. But also sub-saturated nucleation processes (Sassen and Khvorostyanov, 2008) (e.g. deposition nucleation) were found to be an active freezing mechanism under atmospheric conditions. However, the relative importance of the different pathways is not well known at present.

Many species have been identified to act as INP, e.g. mineral dust (e.g., illite, montmorillonite, kaolinite, feldspar), primary biological particles (PBAP), soot, and glassy organics. In laboratory experiments many of these models substances were investigated and their ice forming efficiencies (nucleation temperatures and rates) have been quantified and parameterized (e.g. Murray et al., 2010; Hoose and Moehler, 2012; Atkinson et al., 2013; Wex et al., 2014). However, the type of ambient aerosol particles acting as INP, the importance of their size and the influence of anthropogenically emitted aerosol particles are not well understood. There is still a lack of field measurements concerning the in-situ physio-chemical characterization of atmospheric INP.

In 2011 the Ice Nuclei Research Unit (INUIT) was established with the objective to achieve a more detailed understanding of heterogeneous ice forming processes. The central objective of INUIT is to obtain a better knowledge of ambient aerosol particles serving as INP. Therefore, an ice nucleus counter was connected by means of the counterflow virtual impactor (CVI) technique to online mass spectrometry, and other aerosol measurement techniques, similar to the coupling that had been originally presented by Cziczo et al. (2003) and some years later by Corbin et al. (2012). Corbin et al. (2012) presented measurements from a field study in downtown Toronto (SPORT

2011), where they sampled 196 particles that nucleated ice in a continuous flow diffusion chamber (CFDC) by a pumped CVI (PCVI), and analyzed them with the single particle mass spectrometer ATOFMS. Besides dust, also biomass burning and elemental carbon were identified in these particles. However, statistical limitations hampered the data interpretation. In a similar experimental approach a PCVI was combined with a condensation nucleus counter (CCNC) to investigate cloud droplet residues (Hiranuma et al., 2011; Slowik et al., 2011).

The main components of the present study are the INP counter FINCH (Fast Ice Nucleus Chamber; Bundke et al., 2008, 2010), the IN-PCVI (a pumped CVI (BMI, Model 8100, 2011) operated at new flow settings), and the single particle mass spectrometer ALABAMA (Aircraft-based Laser Ablation Aerosol Mass Spectrometer; Brands et al., 2011). This combination of INP activation, ice particle selection, and INP characterization was first established and technically improved under laboratory conditions. Afterwards the combination was deployed for atmospheric measurements at the Jungfraujoch (JFJ) research station to sample and characterize ambient ice nucleating particles at cloud level.

2 Experimental setup – methods

A schematic of the measurement setup which was realized and operated within INUIT (research project RP 2) is shown in Fig. 1. The IN-PCVI (Sect. 2.1) plays the central role as the ice selecting interface between FINCH (Sect. 2.2) and the aerosol instrumentation consisting of ALABAMA (Sect. 2.3), an impactor for offline scanning electron microscopy (SEM, 2.5), a Condensation Particle Counter (CPC, Sect. 2.4) and an Aerosol Particle Sizer (APS, Sect. 2.4). The CPC, APS, and the IN-PCVI constitute the IN-PCVI system.

AMTD
7, 10585–10617, 2014

2.1 Pumped counterflow virtual impactor – PCVI

The CVI used in this study is a pumped CVI (PCVI) from Brechtel Manufacturing Incorporated (Model 8100, 2011). A first characterization was described in Boulter et al. (2006) and another one was presented by Kulkarni et al. (2011). The CVI technique is used to separate large particles from smaller ones and from the gas that originally surrounded the large particles. This is realized by a counterflow that is directed against the IN-PCVI input flow inside the IN-PCVI. Due to their larger inertia larger particles overcome the counterflow and are thus sampled by the IN-PCVI. In the present setup (Fig. 1) large ice crystals are separated from smaller supercooled droplets and interstitial particles. The IN-PCVI input flow corresponds to the FINCH output flow (illustrated in Fig. 1). The flow rates of the IN-PCVI input flow (F_{IF}), counterflow (F_{CF}) and sample flow (F_{SF}) determine the aerodynamic cut-off diameter ($D_{\mathrm{p50\,\%}}$) of the IN-PCVI. This cut-off diameter represents the particle diameter at which particles are sampled with 50 % efficiency. Particles smaller than the $D_{\mathrm{p50\,\%}}$ are sampled with less than 50 % efficiency. Larger ones are collected with higher efficiency. F_{IF} and F_{CF} are adjusted by the pumped flow (F_{PF}) and the add flow (F_{AF}) (Eqs. 1 and 2). The ice particles that penetrate the counterflow are then transferred into the IN-PCVI sample flow where the water is evaporated in particle-free and dry carrier air.

$$F_{\mathrm{CF}} = F_{\mathrm{AF}} - F_{\mathrm{SF}} \tag{1}$$

$$F_{\mathrm{IF}} = F_{\mathrm{PF}} - F_{\mathrm{CF}} \tag{2}$$

Due to the position of the IN-PCVI between FINCH and the aerosol analysis instrumentation (Fig. 1), the IN-PCVI needs to be operated with different flow settings than the ones used previously (Boulter et al., 2006; Kulkarni et al., 2011). Here the PCVI is operated with a sample flow slightly larger than $1\,\mathrm{L\,min^{-1}}$ and with an input flow in the range of $5\,\mathrm{L\,min^{-1}}$ requiring the determination of the cut-off-characteristics for these specific flow rates. For this purpose a calibration of the $D_{\mathrm{p50\,\%}}$ was done with the setup shown in Fig. 2. Polydisperse polystyrene divinylbenzene (DVB) particles (density = $1.05\,\mathrm{g\,cm^{-3}}$, formula: $(C_{10}H_{10} \cdot C_8H_8)x$, Duke Scientific Corporation, now Thermo Scientific) with diameters in a range of 2 to 120 µm (aerodynamic size: Fig. 3) were used as well-defined reference aerosol particles. The polystyrene DVB particles were dispersed manually by a powder dispenser (pushing the balloon which is shown in Fig. 2) and pumped into the IN-PCVI at a prescribed input flow rate of 4, 4.5, or 5 L min^{-1}. For several combinations of input flow rate, counterflow rate (0, 2, 2.5, 3, 3.5 L min^{-1}) and sample flow rate (1, 1.3, 2, and 3 L min^{-1}), at which the IN-PCVI was operated (Table 1), the number size distribution of the test aerosol was measured with an APS. The number size distribution measured with the counterflow being switched off was taken as reference. It was normalized to a maximum of 1 and all cut-off size distributions (i.e., F_{CF} switched on) measured for the same inlet and sample flow were scaled to match the right branch of the reference size distribution. This approach was chosen to minimize the error due to size-dependent particle losses in the inlet region of the IN-PCVI. The calibration runs were repeated several times for averaging the aerodynamic size distribution and thus to minimize the error due to the manual dispersion of the calibration aerosol.

The calibration curves of the most common sample and input flow settings of the INUIT-JFJ/CLACE 2013 campaign (Run 4–7, Table 1) are illustrated in Figs. 3 and 4. Figure 3 shows the normalized APS measured aerodynamic size distribution, here for a fixed F_{IF} and F_{SF}, while F_{CF} is varied. As expected, for larger counterflows the cut-off is shifted to larger sizes. The transmission efficiency (TE, sampling efficiency of particles of a certain size passing the IN-PCVI) is defined by the ratio of the normalized sample flow concentration N_{out} with counterflow switched on and the normalized reference concentration N_{in} ($F_{CF} = 0$) (Eq. 3).

$$\mathrm{TE} = \frac{N_{out}(d_p)_{norm.}}{N_{in}(d_p)_{norm.}} \qquad (3)$$

Figure 4 shows the transmission efficiency curves for the measurements shown in Fig. 3. The vertical dashed lines mark the resulting cut-off-diameter, $D_{p50\,\%}$. It can be seen that with increasing F_{CF} from 0.5 to 3.5 L min^{-1} the $D_{p50\,\%}$ increases from 5 to

AMTD
7, 10585–10617, 2014

6.5 µm. The behavior of the $D_{p50\%}$ was also studied for different input and sample flows. The resulting $D_{p50\%}$ for all flow variations were in a range between 5.2 and 8.4 µm (Fig. 5). It is evident that a change of the $D_{p50\%}$ is most sensitiv to a change of F_{IF} compared to a change of F_{SF} or F_{CF} (slopes of regressions for the chosen flow regime are shown in Fig. 5a–c). In Fig. 5a, $D_{p50\%}$ results determined by Kulkarni et al. (2011) are displayed for comparison. Since F_{IF} in our experiments is lower ($F_{IF} = 5\,\mathrm{L\,min^{-1}} < F_{IF(Kulkarni)} = 6.7\,\mathrm{L\,min^{-1}}$), the absolute $D_{p50\%}$ values are higher. Nevertheless, the same relative change in $D_{p50\%}$ (same slope) is found for the two F_{IF} settings.

The cut-off diameters for the new flow parameters (Table 1) represent an extended characterization of the commercial PCVI from Brechtel Inc., clearly showing that this device is working properly in the flow regime required for the operation of the IN-PCVI during the INUIT-JFJ/CLACE 2013 field campaign.

2.2 Fast Ice Nucleus Chamber (FINCH)

FINCH was developed and built at the Goethe University of Frankfurt. It is an in situ counter for ice nucleating particles, which is operated by mixing air flows with different humidity and temperature to achieve supersaturation (with respect to water (S_{wat_F}) and with respect to ice (S_{ice_F})) (Bundke et al., 2008). The main component of the device is a temperature-controlled, stainless steel growth chamber with a length of 0.8 m that can be cooled down to −65 °C. Sampled aerosol particles are activated and grow to macroscopic ice particles or supercooled droplets depending on the temperature (T_F) and supersaturation (S_{ice_F}) inside the chamber.

Depending on the mixed air flow rate the aerosol particles typically need ∼ 10 s to pass the chamber. The (grown) particles are counted in an optical particle counter mounted directly below the chamber (BIO-IN-OPC; Bundke et al., 2010). Based on scattering properties a distinction between water droplets and ice particles is possible (P44/P11 ratio of the scattering matrix; Hu et al., 2003). The current setup of the detector consists of a 405 nm laser, which stimulates the particles to fluoresce as well. In this study the outlet of the BIO-IN-OPC was directly connected to the IN-PCVI.

After several hours of operation the measurements with FINCH are interrupted for a short heating period to melt the ice that had built up in the inlet and thus resulted in a reduced or plugged flow. After every heating period the saturation ratio inside FINCH is automatically re-established to the set value, which can take up to an hour. During operation $S_{\mathrm{ice}_\mathrm{F}}$ is adjusted continuously as a consequence of changing ambient temperature and relative humidity.

2.3 Aircraft-based laser ablation aerosol mass spectrometer (ALABAMA)

ALABAMA is a single particle laser ablation instrument to detect the chemical composition, mixing state and size of aerosol particles in a range from 150–900 nm (Brands et al., 2011). It was built and characterized at the Max Planck Institute for Chemistry (MPIC) Mainz. The particles are detected and sized by two continuous lasers at a wavelength of 405 nm (InGaN Blu-Ray laser). Thereafter, a 266 nm wavelength pulsed Nd-YAG-laser is used to evaporate the aerosol particles and ionize the components. A bipolar, Z-shaped time-of-flight mass spectrometer (Tofwerk) generally detects positive and negative ions. During the INUIT-JFJ/CLACE 2013 campaign only positive ions were detected due to technical issues. It is used to measure the chemical composition of FINCH-detected INP, which are separated, sampled and released by the IN-PCVI.

2.4 Microphysical aerosol instrumentation

For a microphysical characterization of the INP a condensation particle counter (CPC TSI 3010) and an aerodynamic particle sizer (APS TSI 3321) were connected downstream the IN-PCVI. The CPC measures the number concentration of particles that are larger than 0.01 µm in diameter.

AMTD
7, 10585–10617, 2014

The APS measures the aerodynamic number size distribution of aerosol particles in the size range between 0.5 and 20 µm. The sizing is done by a time-of-flight measurement between two laser beams. The IN-PCVI in combination with CPC and APS are called IN-PCVI system in the following.

2.5 Scanning electron microscopy (SEM)

Ice-nucleating particles were collected downstream the IN-PCVI by a two-stage impactor system (50 % cut-off aerodynamic diameters 1.0 and 0.1 µm, respectively) and were analyzed offline by scanning electron microscopy and energy-dispersive X-ray fluorescence (EDX). Particles were collected on transmission electron microscopy grids and elemental boron. The samples were analyzed in a scanning electron microscope (FEI Quanta 200 FEG, FEI, Eindhoven, the Netherlands) with attached energy-dispersive X-ray fluorescence microanalysis (EDX, EDAX, Tilburg, the Netherlands) to characterize the particles with regard to their chemical composition, morphology, size, internal mixing state and electron beam stability (volatility). Based on criteria of chemical composition, morphology mixing state and beam stability, particles were sorted into ten singular classes (carbonaceous, sulfate and other secondary aerosol, soot, sea-salt, Ca-rich, metal oxide, silicate, Pb-bearing, droplets, and other particles). For details on the particle classes, the reader is referred to Worringen et al. (2014). Due to their low abundance, in the present work sea-salt and Pb-bearing particles are subsummarized with all other unclassified particles into the so-called "other" class.

2.6 Test measurements in the laboratory

Prior to field operation, the volume flow management of the combination of FINCH, the IN-PCVI and several aerosol particle instruments was set up and tested during two technical laboratory campaigns in Frankfurt and Leipzig. Since each component has its own standalone flow system, the main concern was to adapt and couple the flows and to ensure a smooth and efficient transition of the sample from one component

AMTD
7, 10585–10617, 2014

to the following one. As a main result of these tests, the FINCH closed loop had to be switched off and the FINCH aerosol flow had to be directly controlled by the IN-PCVI pump flow. This led to stable pressure conditions inside the coupled FINCH + IN-PCVI flow system. Additionally, it was found that changes in the IN-PCVI – FINCH flows caused fluctuations in the supersaturation of FINCH, which sometimes resulted in a frozen inlet and thus blocking of the growth chamber. Therefore, the FINCH – IN-PCVI flows were was kept constant during single measurement runs.

2.7 Atmospheric measurements at the high Alpine research station Jungfraujoch

The combination of INP activation and detection (FINCH), separation/preparation (IN-PCVI), and characterization (aerosol instrumentation) was deployed in January/February 2013 during the INUIT-JFJ/CLACE-2013 joint measurement field campaign (Schneider et al., 2014) at the Sphinx Laboratory of the high Alpine research station Jungfraujoch (JFJ, Bernese Alps, Switzerland, 3580 m a.s.l.). The combination of FINCH, IN-PCVI, and aerosol instruments was deployed at this site to sample aerosol particles inside mixed-phase or, sometimes, even entirely glaciated clouds, where supercooled drops and small ice particles were evaporated during collection by heated total aerosol inlet (operated by Paul Scherrer Institute, Villigen; Weingartner et al., 1999). Also ambient background aerosol particles, which are present during cloud free time periods, are sampled at these altitude that are realistic for the mixed-phase cloud formation at mid latitudes.

AMTD
7, 10585–10617, 2014

3 Results

3.1 Proof of principle for the FINCH + IN-PCVI coupling

The main focus of this work was to verify the feasibility of the FINCH + IN-PCVI coupling for the physical and chemical characterization of atmospheric INP by different aerosol sensors attached to the IN-PCVI.

A stability criterion of the adjusted ice saturation ratio inside FINCH needed to be specified to ensure the data analysis under constant measurement conditions. Fluctuations in the FINCH saturation ratio may lead to different conditions under which freezing occurs and thus to differences in the final sizes to which the ice particles grow. Therefore, only measurement periods in which the ice saturation ratio varied by less than 1 % (relatively) within 300 s were used for further analysis. This criterion is somewhat arbitrary, but appeared to effectively eliminate the poorly defined activation periods while leaving sufficient amount of data points for the proof-of-principle study.

During the INUIT-JFJ/CLACE-2013 campaign the complete coupled system of FINCH, IN-PCVI and aerosol instruments was connected to the heated total aerosol inlet sampling line to investigate the ice activation ability of ambient aerosol particles and during cloud periods also of cloud ice particle residuals and cloud droplet residuals. For this purpose FINCH was operated in the temperature range between −18 and −26 °C and at ice saturation ratios between 1.05 and 1.5. Figure 6 shows the $T_F - S_{ice_F}$ pairs (10 min averages) from the campaign that remain after applying the stability criterion. Moreover, the corresponding lines of the calculated water saturation ratio (0.90 to 1.25 in 0.05 steps) are indicated. The majority of the 10 min periods used in the following discussion are located in the water supersaturated region ($S_{wat_F} > 1.0$) when immersion freezing is the dominant heterogeneous ice nucleation mechanism inside FINCH. Only a few data points are below $S_{wat_F} = 1.0$ when ice activation in FINCH is limited to deposition nucleation and immersion freezing in highly concentrated solution droplets (Wex et al., 2014) only. Figure 7 shows a log-log scatterplot of the number concentration of ice nucleating particles measured by the FINCH optics ($N_{INP_{FINCH}}$) and

AMTD
7, 10585–10617, 2014

measured by the IN-PCVI CPC ($N_{INP_{IN\text{-}PCVI}}$, same 10 min averages). The data points are subdivided into 3 classes with regard to the prevailing FINCH water saturation ratio:

$$S_{wat_F} < 1.0 \text{ (squares)}, \quad 1.0 < S_{wat_F} < 1.1 \text{ (circles) and} \quad 1.1 < S_{wat_F} < 1.2 \text{ (crosses).}$$

The 1 : 1 line indicated in Fig. 7 shows that there exists a very close correlation between $N_{INP_{FINCH}}$ and $N_{INP_{IN\text{-}PCVI}}$ for $S_{wat_F} < 1.0$ (squares), which implies that the residue of each ice particle grown in FINCH is transferred with high efficiency through the IN-PCVI and all other particles exiting FINCH (supercooled droplets, unactivated particles) are diverted into the F_{PF} of the IN-PCVI. With increasing water saturation ratio, however, $N_{INP_{IN\text{-}PCVI}}$ concentration exceeds $N_{INP_{FINCH}}$. Since it is not likely that more ice nucleating particles exist after the IN-PCVI than there were ice particles counted after FINCH, the most probable explanation is that some liquid supercooled droplets that are formed in FINCH reach the same size as the ice particles at higher saturation. Thus, they cannot be pre-segregated by the IN-PCVI and become erroneously counted and sampled as INP. In order to estimate the magnitude of this effect, power regressions (with an exponent equal 1) were calculated for each class and plotted in Fig. 7. These indicate contribution of large droplet residuals 0, 45, and 63 % for the intended INP sampling with respect to the three S_{wat_F} classes.

Table 2 gives a more detailed verification of the droplet contamination effect. Again power regressions are derived from the $N_{INP_{FINCH}}$ to $N_{INP_{IN\text{-}PCVI}}$ relationship but now separately for a S_{wat_F} increment of 0.01. The desired regression close to 1 is only achieved for $S_{wat_F} \leq 1.01$, which denotes an ice saturation between 1.21 and 1.3 for the adjusted temperatures. However, the uncertainty of the regression slope includes 1 still for a $S_{wat_F} \leq 1.06$ ($1.21 < S_{ice_F} < 1.34$). Accepting a ratio of one drop residual out of three $INP_{IN\text{-}PCVI}$ would allow to take into account all measurements up to $S_{wat_F} \leq 1.08$ ($1.21 < S_{ice_F} < 1.34$). For all INP results obtained by the coupled system these limitations and uncertainties have to be taken into account.

AMTD
7, 10585–10617, 2014

3.2 First measurements of INP properties

Having proven the feasibility and discussed the operational limitations of the FINCH + IN-PCVI coupling, now first exemplary results of INP properties obtained with this experimental setup during the INUIT-JFJ/CLACE-2013 campaign are presented. Identical to the experimental setup described in Sect. 3.1 ambient particles as well as residues of supercooled drops or ice particles in the presence of clouds were sampled by the heated total aerosol inlet, to which the combination of FINCH, IN-PCVI, and aerosol sensors was connected to. During all measurements at the JFJ the IN-PCVI cut-off diameter was adjusted in the characterized range, which is shown in Fig. 5a–c. Figure 8 shows an INP time series from a 4 h case study on 9 February 2013. The data points are again 10 min mean values and meet the above described criterion of the FINCH saturation ratio varying less than 1 % in 300 s. Within this period T_F was adjusted in a range from −21 to −23.5 °C and S_{ice_F} to ~ 1.1, respectively. Thus, FINCH was operated at water sub-saturated conditions, i.e. deposition nucleation and/or immersion freezing of highly concentrated solutions are the prevailing heterogeneous nucleation mechanisms inside FINCH. Consistent with the findings in Sect. 3.1, the FINCH and IN-PCVI INP concentrations agree very well in this case study increasing from 5 to 25 L^{-1}. The reason for the increase of the INP concentration by a factor of 5 within 3 h is not clear, but a decisive change in the air mass can be ruled out.

Another measure for the INP number concentration is inferred from integrating the INP number size distribution measured by the APS (Fig. 8). The lower size detection limit of the APS is 0.55 µm, i.e., the APS $N_{INP_{IN\text{-}PCVI}}$ refers to all $INP_{IN\text{-}PCVI}$ larger than this diameter. The variation of the concentration of these large INP in time shows the same increasing trend but on a substantially lower level between 0 to 4 L^{-1}, which is a factor of 7 below the values of the total INP concentration. Hence, it can be concluded that only 13 % of the sampled INP are larger than 0.55 µm and the majority of the INP (87 %) are smaller for the situation encountered in this case study. Tests of the reduced counting efficiency in the lower APS channels (555–700 nm) showed only

AMTD
7, 10585–10617, 2014

a weak (1–5 %) influence on the integrated APS number concentration. Nevertheless, this technical uncertainty should be kept in mind.

For the examined time period the ambient background particle concentration was roughly between 1100–2900 cm^{-3} (measured also at the heated inlet sample line by a PSI operated CPC, TSI 3772), which leads to an ambient INP fraction of approx. 2×10^{-5}. Over the whole campaign the INP fraction was found to be between 1×10^{-6} and 4×10^{-5} (for ice saturation ratios between 1.05 and 1.35 and FINCH temperature between −18 and −25 °C). This agrees well to other atmospheric INP number concentration studies (Pruppacher and Klett, 1997; Mason, 1971; Rogers et al., 1998; Eidhammer et al., 2009; DeMott et al., 2010). Nevertheless, the INP concentration is most of the time in the lower range compared to these other studies but a more comprehensive comparison of the measured INP concentrations observed with FINCH during INUIT-JFJ 2013 with other published INP data will be given by Frank et al. (2014). However, reasons for the rather low INP concentrations presented here could be the restriction to rather low saturation conditions inside FINCH for the coupling with the IN-CVI or the high and remote location of the measurement site with low ambient aerosol particle number concentration.

Figure 9 presents a frequency distribution of INP sizes measured by the APS (dashed line) downstream of the IN-PCVI. Only APS measurements are included which are carried out at $S_{wat_F} \leq 1.01$ in order to be sure that only INP are sampled without contamination by large drop residuals. The frequency distribution decreases with a shallow slope towards super-micrometer diameters, which confirms previous measurements showing that large aerosol particles are more effective INP (Mertes et al., 2007). This finding is supported by the comparison with a frequency distribution of ambient aerosol particle sizes (solid line in Fig. 9), which decreases more steeply with increasing particle size. The latter distribution was measured with an Optical Particle Sizer (OPS, TSI 3330) and normalized to the APS distribution at 0.55 µm.

The combination of FINCH + IN-PCVI with the single particle mass spectrometer ALABAMA for online chemical analysis of INP was one of the main objectives of this study. However, it turned out to be the most ambitious goal due to the limited measurement time at low and constant water saturation conditions in FINCH, and due to an insufficient particle detection efficiency of ALABAMA. Only seven single particle mass spectra of INP were recorded with ALABAMA during the INUIT-JFJ/CLACE-2013 campaign, which makes a statistical or cloud event differentiated analysis impossible. The few ALABAMA INP mass spectra show mainly organic material but also other elements as Li, Na, Al, Fe, and K, that might be related to biological particles, biomass burning, or mineral dust particles coated with organic matter as the main INP components (see example in Fig. 10). These compositions are similar to those detected by ALABAMA in ice particle residuals during the same project (Schmidt et al., 2014).

Furthermore, impactor samples were taken downstream of the IN-PCVI and analyzed offline by electron microscopy. A detailed discussion of the SEM results is presented by Worringen et al. (2014).

4 Summary and conclusions

The combination of an ice nucleus counter (FINCH), a counterflow virtual impactor (IN-PCVI), and different instruments for physical and chemical aerosol particle characterization was set up, tested, characterized, and deployed for the first time to investigate the properties of ice nucleating particles under free tropospheric conditions. This included operation of a single particle mass spectrometer, ALABAMA, for chemical INP analysis.

The cut-off behavior of the IN-PCVI was successfully determined for the specific flow settings required for the instrument combination. Feasibility and functionality of the instrument combination were proven in the framework of the INUIT-JFJ/CLACE 2013 field measurements. It was found that an important prerequisite for a successful coupling of FINCH and the IN-PCVI are stable ice saturation ratios inside the IN counter. A relative change of less than 1 % in S_{ice_F} within 300 s was therefore chosen as a criterion for the data analysis. $\text{INP}_{\text{FINCH}}$ and $\text{INP}_{\text{IN-PCVI}}$ number concentration measurements

AMTD
7, 10585–10617, 2014

showed an excellent agreement for water saturation ratios ≤ 1.01 ($1.21 < S_{ice_F} < 1.3$). This implies that ice particles nucleated in FINCH are efficiently separated by the IN-PCVI from the interstitial particles and supercooled droplets that are also present at the FINCH outlet, and that consequently only INP are selected by the IN-PCVI for further analysis. At higher water saturation ratios higher INP concentrations were measured with the IN-PCVI CPC than with the FINCH optics, which may be attributed to supercooled drops growing into the same size range as the ice particles and can therefore not be rejected by the counterflow. This effect is estimated to result in an overestimation of INP concentrations by about 25 % for FINCH water saturation ratios up to 1.08 ($1.21 < S_{ice_F} < 1.34$).

Ambient INP properties were inferred from the measurements carried out during the INUIT-JFJ/CLACE 2013 field campaign. Restricting the considered measurements to water saturation ratios ≤ 1.0, i.e., considering deposition nucleation and/or immersion freezing of highly concentrated solutions, INP concentrations of up to 40 L^{-1} were measured (S_{ice_F} between 1.0 and 1.3, temperatures between −15 and −28 °C) over the campaign duration. In a 4 h case study 87 % of the INP were found to be smaller than 0.55 µm. From the shape of the frequency distribution of INP diameters it can be concluded that the ice nucleating efficiency increases with particle size.

The combination of FINCH + IN-PCVI + ALABAMA resulted in 7 mass spectra of INP, which cannot be statistically evaluated, but represent a successful proof-of-concept for the system. A clear need to improve the counting efficiency of the FINCH + IN-PCVI + ALABAMA combination has to be stated when deploying the system in environments with low INP concentrations. However, for laboratory applications and use in environments with high INP concentrations, the FINCH + IN-PCVI + ALABAMA combination can already by applied in the current development stage.

Acknowledgements. This project is funded by the German Research Foundation (Research Unit INUIT, FOR 1525, grants STR 453/7-1, BU 1432/4-1, SCHN1138/2-1 and EB 383/3-1 and DFG grant ME 3534/1-2). The authors thank the International Foundation High Altitude Research Station Jungfraujoch and Gornergrat (HFSJG). We thank T. Klimach for help with the ALABAMA operation during the JFJ campaign. Also, we thank Thomas Conrath for his intensive technical support.

References

Ansmann, A., Tesche, M., Seifert, P., Althausen, D., Engelmann, R., Fruntke, J., Wandinger, U., Mattis, I., and Mueller, D.: Evolution of the ice phase in tropical altocumulus: SAMUM lidar observations over Cape Verde, J. Geophys. Res.-Atmos., 114, D17208, doi:10.1029/2008JD011659, 2009. 10588

Atkinson, J. D., Murray, B. J., Woodhouse, M. T., Whale, T. F., Baustian, K. J., Carslaw, K. S., Dobbie, S., O'Sullivan, D., and Malkin, T. L.: Erratum: The importance of feldspar for ice nucleation by mineral dust in mixed-phase clouds, Nature, 500, p. 490, doi:10.1038/nature12384, 2013. 10588

Boulter, J. E., Cziczo, D. J., Middlebrook, A. M., Thomson, D. S., and Murphy, D. M.: Design and performance of a pumped counterflow virtual impactor, Aerosol Sci. Tech., 40, 969–976, doi:10.1080/02786820600840984, 2006. 10590

Brands, M., Kamphus, M., Böttger, T., Schneider, J., Drewnick, F., Roth, A., Curtius, J., Voigt, C., Borbon, A., Beekmann, M., Bourdon, A., Perrin, T., and Borrmann, S.: Characterization of a newly developed Aircraft-Based Laser Ablation Aerosol Mass Spectrometer (ALABAMA) and first field deployment in urban pollution plumes over Paris during MEGAPOLI 2009, Aerosol Sci. Tech., 45, 46–64, doi:10.1080/02786826.2010.517813, 2011. 10589, 10593

Bundke, U., Nillius, B., Jaenicke, R., Wetter, T., Klein, H., and Bingemer, H.: The Fast Ice Nucleus Chamber FINCH, Atmos. Res., 90, 180–186, doi:10.1016/j.atmosres.2008.02.008, 2008. 10589, 10592

Bundke, U., Reimann, B., Nillius, B., Jaenicke, R., and Bingemer, H.: Development of a Bioaerosol single particle detector (BIO IN) for the Fast Ice Nucleus CHamber FINCH, Atmos. Meas. Tech., 3, 263–271, doi:10.5194/amt-3-263-2010, 2010. 10589, 10592

Corbin, J., Rehbein, P., Evans, G., and Abbatt, J.: Combustion particles as ice nuclei in an urban environment: evidence from single-particle mass spectrometry, Atmos. Environ., 51, 286–292, doi:10.1016/j.atmosenv.2012.01.007, 2012. 10588

Cziczo, D. J., DeMott, P. J., Brock, C., Hudson, P. K., Jesse, B., Kreidenweis, S. M., Prenni, A. J., Schreiner, J., Thomson, D. S., and Murphy, D. M.: A method for single particle mass spectrometry of ice nuclei, Aerosol Sci. Tech., 37, 460–470, doi:10.1080/02786820300976, 2003. 10588

de Boer, G., Morrison, H., Shupe, M. D., and Hildner, R.: Evidence of liquid dependent ice nucleation in high-latitude stratiform clouds from surface remote sensors, Geophys. Res. Lett., 38, L01803, doi:10.1029/2010GL046016, 2011. 10588

DeMott, P. J., Prenni, A. J., Liu, X., Kreidenweis, S. M., Petters, M. D., Twohy, C. H., Richardson, M. S., Eidhammer, T., and Rogers, D. C.: Predicting global atmospheric ice nuclei distributions and their impacts on climate, P. Natl. Acad. Sci. USA, 107, 11217–11222, doi:10.1073/pnas.0910818107, 2010. 10599

DeMott, P. J., Möhler, O., Stetzer, O., Vali, G., Levin, Z., Petters, M. D., Murakami, M., Leisner, T., Bundke, U., Klein, H., Kanji, Z. A., Cotton, R., Jones, H., Benz, S., Brinkmann, M., Rzesanke, D., Saathoff, H., Nicolet, M., Saito, A., Nillius, B., Bingemer, H., Abbatt, J., Ardon, K., Ganor, E., Georgakopoulos, D. G., and Saunders, C.: Resurgence in ice nuclei measurement research, B. Am. Meteorol. Soc., 92, 1623–1635, doi:10.1175/2011BAMS3119.1, 2011. 10588

Eidhammer, T., DeMott, P. J., and Kreidenweis, S. M.: A comparison of heterogeneous ice nucleation parameterizations using a parcel model framework, J. Geophys. Res.-Atmos., 114, D06202, doi:10.1029/2008JD011095, 2009. 10599

Hiranuma, N., Kohn, M., Pekour, M. S., Nelson, D. A., Shilling, J. E., and Cziczo, D. J.: Droplet activation, separation, and compositional analysis: laboratory studies and atmospheric measurements, Atmos. Meas. Tech., 4, 2333–2343, doi:10.5194/amt-4-2333-2011, 2011. 10589

Hoose, C. and Möhler, O.: Heterogeneous ice nucleation on atmospheric aerosols: a review of results from laboratory experiments, Atmos. Chem. Phys., 12, 9817–9854, doi:10.5194/acp-12-9817-2012, 2012. 10588

Hu, Y., Yang, P., Lin, B., Gibson, G., and Hostetler, C.: Discriminating between spherical and non-spherical scatterers with lidar using circular polarization: a theoretical study, J. Quant. Spectrosc. Ra., 79, 757–764, doi:10.1016/S0022-4073(02)00320-5, 6th International Conference on Electromagnetic and Light Scattering by Nonspherical Particles, Univ. Florida, Gainesville, FL, 4–8 March 2002, 2003. 10592

Kulkarni, G., Pekour, M., Afchine, A., Murphy, D. M., and Cziczo, D. J.: Comparison of experimental and numerical studies of the performance characteristics of a pumped counterflow virtual impactor, Aerosol Sci. Tech., 45, 382–392, doi:10.1080/02786826.2010.539291, 2011. 10590, 10592, 10612

Mason, B. J.: The Physics of Clouds, Clarenson Press, Oxford, 1971. 10599

Mertes, S., Verheggen, B., Walter, S., Connolly, P., Ebert, M., Schneider, J., Bower, K. N., Cozic, J., Weinbruch, S., Baltensperger, U., and Weingartner, E.: Counterflow virtual impactor based collection of small ice particles in mixed-phase clouds for the physico-chemical characterization of tropospheric ice nuclei: sampler description and first case study, Aerosol Sci. Tech., 41, 848–864, doi:10.1080/02786820701501881, 2007. 10599

Murray, B. J., Wilson, T. W., Dobbie, S., Cui, Z., Al-Jumur, S. M. R. K., Moehler, O., Schnaiter, M., Wagner, R., Benz, S., Niemand, M., Saathoff, H., Ebert, V., Wagner, S., and Kaercher, B.: Heterogeneous nucleation of ice particles on glassy aerosols under cirrus conditions, Nat. Geosci., 3, 233–237, doi:10.1038/NGEO817, 2010. 10588

Murray, B. J., O'Sullivan, D., Atkinson, J. D., and Webb, M. E.: Ice nucleation by particles immersed in supercooled cloud droplets, Chem. Soc. Rev., 41, 6519–6554, doi:10.1039/C2CS35200A, 2012. 10588

Pruppacher, H. and Klett, J.: Microphysics of Clouds and Precipitation, Kluwer, Dordrecht, The Netherlands, ISBN: 0-7923-4211-9, 1997. 10588, 10599

Rogers, D. C., DeMott, P. J., Kreidenweis, S. M., and Chen, Y.: Measurements of ice nucleating aerosols during SUCCESS, Geophys. Res. Lett., 25, 1383–1386, doi:10.1029/97GL03478, 1998. 10599

Sassen, K. and Khvorostyanov, V. I.: Cloud effects from boreal forest fire smoke: evidence for ice nucleation from polarization lidar data and cloud model simulations, Environ. Res. Lett., 3, 025006, doi:10.1088/1748-9326/3/2/025006, 2008. 10588

Slowik, J. G., Cziczo, D. J., and Abbatt, J. P. D.: Analysis of cloud condensation nuclei composition and growth kinetics using a pumped counterflow virtual impactor and aerosol mass spectrometer, Atmos. Meas. Tech., 4, 1677–1688, doi:10.5194/amt-4-1677-2011, 2011. 10589

Vali, G., DeMott, P., Möhler, O., and Whale, T. F.: Ice nucleation terminology, Atmos. Chem. Phys. Discuss., 14, 22155–22162, doi:10.5194/acpd-14-22155-2014, 2014. 10588

Weingartner, E., Nyeki, S., and Baltensperger, U.: Seasonal and diurnal variation of aerosol size distributions ($10 < D < 750$ nm) at a high-alpine site (Jungfraujoch 3580 m a.s.l.), J. Geophys. Res.-Atmos., 104, 26809–26820, doi:10.1029/1999JD900170, 1999. 10595

Westbrook, C. D. and Illingworth, A. J.: Evidence that ice forms primarily in supercooled liquid clouds at temperatures > -27 °C, Geophys. Res. Lett., 38, L14808, doi:10.1029/2011GL048021, 2011. 10588

AMTD
7, 10585–10617, 2014

Sampling of ambient ice nucleating particles

L. P. Schenk et al.

Wex, H., DeMott, P. J., Tobo, Y., Hartmann, S., Rösch, M., Clauss, T., Tomsche, L., Niedermeier, D., and Stratmann, F.: Kaolinite particles as ice nuclei: learning from the use of different kaolinite samples and different coatings, Atmos. Chem. Phys., 14, 5529–5546, doi:10.5194/acp-14-5529-2014, 2014. 10588, 10596

Worringen, A., Kandler, K., Benker, N., Dirsch, T., Weinbruch, S., Mertes, S., Schenk, L., Kästner, U., Frank, F., Nillius, B., Bundke, U., Rose, D., Curtius, J., Kupiszewski, P., Weingartner, E., Schneider, J., Schmidt, S., and Ebert, M.: Single-particle characterization of ice-nucleating particles and ice particle residuals sampled by three different techniques, Atmos. Chem. Phys. Discuss., 14, 23027–23073, doi:10.5194/acpd-14-23027-2014, 2014. 10594, 10600

Table 1. Flow setup of the IN-PCVI (counterflow (F_{CF}), input flow (F_{IF}), sample flow (F_{SF})) resulting in different cut-off-diameters ($D_{p50\,\%}$).

Run	F_{CF} (L min^{-1})	F_{IF} (L min^{-1})	F_{SF} (L min^{-1})	$D_{p50\,\%}$ (µm)
1	3	5	1	5.6
2	3	5	2	6.5
3	3	5	3	7.9
4	2	5	1.3	5.2
5	2.5	5	1.3	6
6	3	5	1.3	6.2
7	3.5	5	1.3	6.5
8	3	4	1.3	8.4
9	3	4.5	1.3	7.8
10	3	5	1.3	6.2

AMTD
7, 10585–10617, 2014

Sampling of ambient ice nucleating particles

L. P. Schenk et al.

AMTD
7, 10585–10617, 2014

Table 2. Slope a of the $N_{\mathrm{INP}_{\mathrm{IN\text{-}PCVI}}} - N_{\mathrm{INP}_{\mathrm{IN\text{-}PCVI}}}$ scatter plot regression depending on the considered water saturation range, the standard deviation (SD) of *a*, the derived relative droplet contaminations (RDC) and corresponding ice saturation ratios for the investigated temperature range.

S_{wat_F} range	a	SD(a)	RDC (%)	$S_{\mathrm{ice}_F}(-18\,^\circ\mathrm{C}) - S_{\mathrm{ice}_F}(-26\,^\circ\mathrm{C})$
≤ 1	0.94	0.05	0	1.2–1.3
≤ 1.01	1.03	0.22	3	1.21–1.31
≤ 1.02	1.12	0.26	12	1.22–1.33
≤ 1.03	1.09	0.22	9	1.24–1.34
≤ 1.04	1.08	0.2	8	1.25–1.35
≤ 1.05	1.13	0.2	13	1.26–1.37
≤ 1.06	1.17	0.18	17	1.27–1.38
≤ 1.07	1.18	0.17	18	1.28–1.39
≤ 1.08	1.24	0.14	24	1.3–1.41
≤ 1.09	1.26	0.13	26	1.31–1.42
≤ 1.1	1.32	0.1	32	1.32–1.43
≤ 1.2	1.53	0.07	53	1.44–1.56

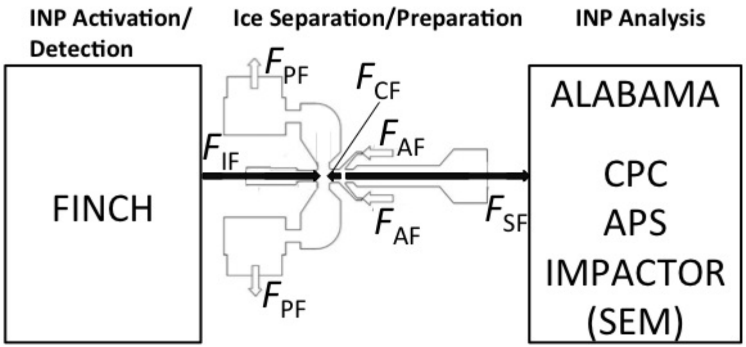

Figure 1. Schematics of the coupled FINCH – IN-PCVI – analysis setup. FINCH activates the INP and counts the grown ice crystals. The IN-PCVI separates these ice particles from non-activated aerosol particles and smaller supercooled droplets, which are also formed inside FINCH. The released INP are transferred to the aerosol sensors for chemical and physical analysis. Flows inside the IN-PCVI are illustrated by arrows and described in the text.

AMTD
7, 10585–10617, 2014

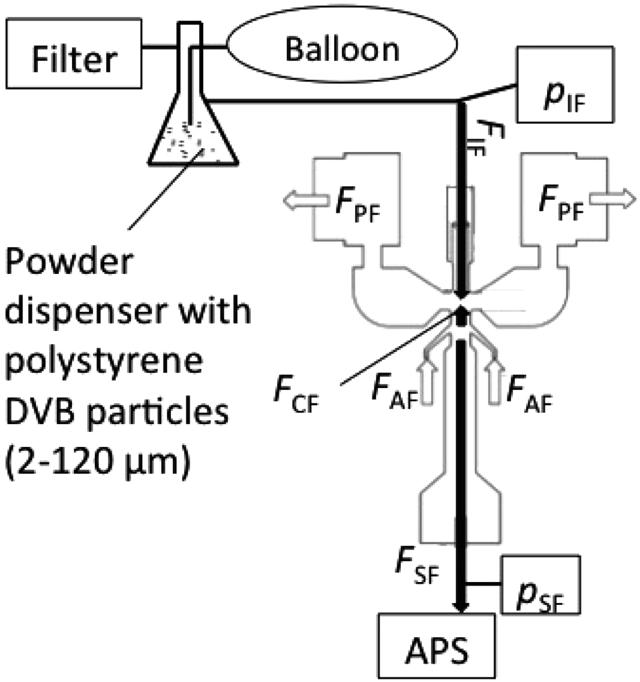

Figure 2. Sketch of the measurement setup for the IN-PCVI $D_{p50\,\%}$ characterization. A pump bottle is used to disperse polystyrene DVP particles (2–120 µm). The APS of the IN-PCVI system connected downstream of the IN-PCVI measured the reference size distribution (F_{CF} switched off) and the size distribution when the counterflow was switched on. The pressure is measured up- and downstream the IN-PCVI to ensure stable flow conditions (p_{IF} and p_{SF}).

AMTD
7, 10585–10617, 2014

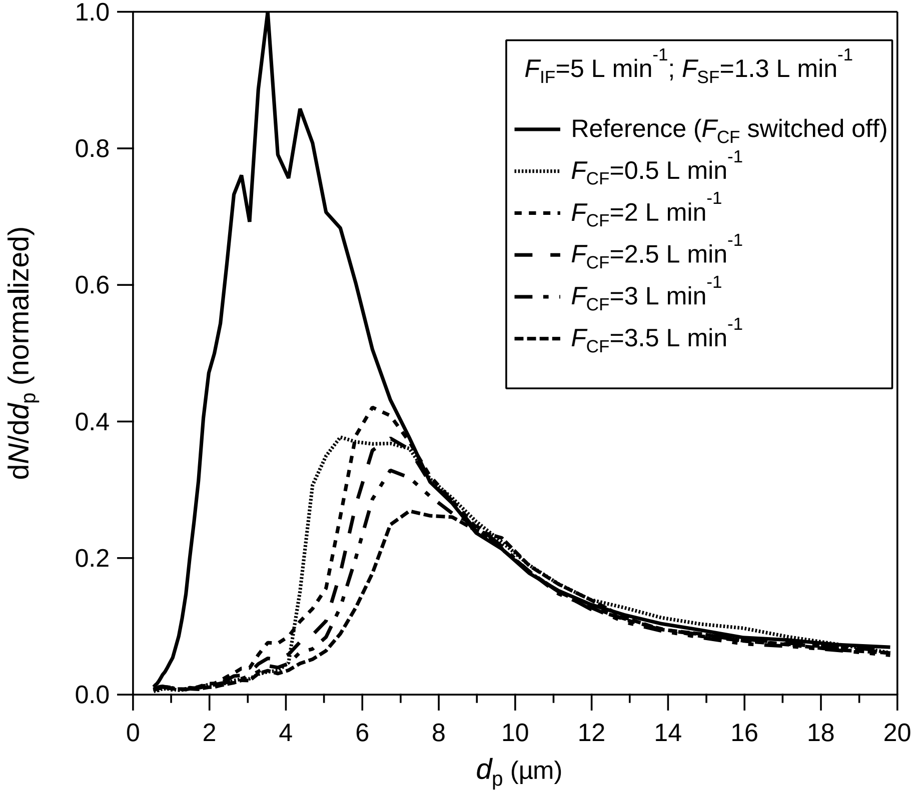

Figure 3. Polystyrene DVB reference number size distribution (solid line) and number size distributions at different counterflows (see legend). All number size distributions were measured by the APS and were normalized to a maximum of 1.

AMTD
7, 10585–10617, 2014

Sampling of ambient ice nucleating particles

L. P. Schenk et al.

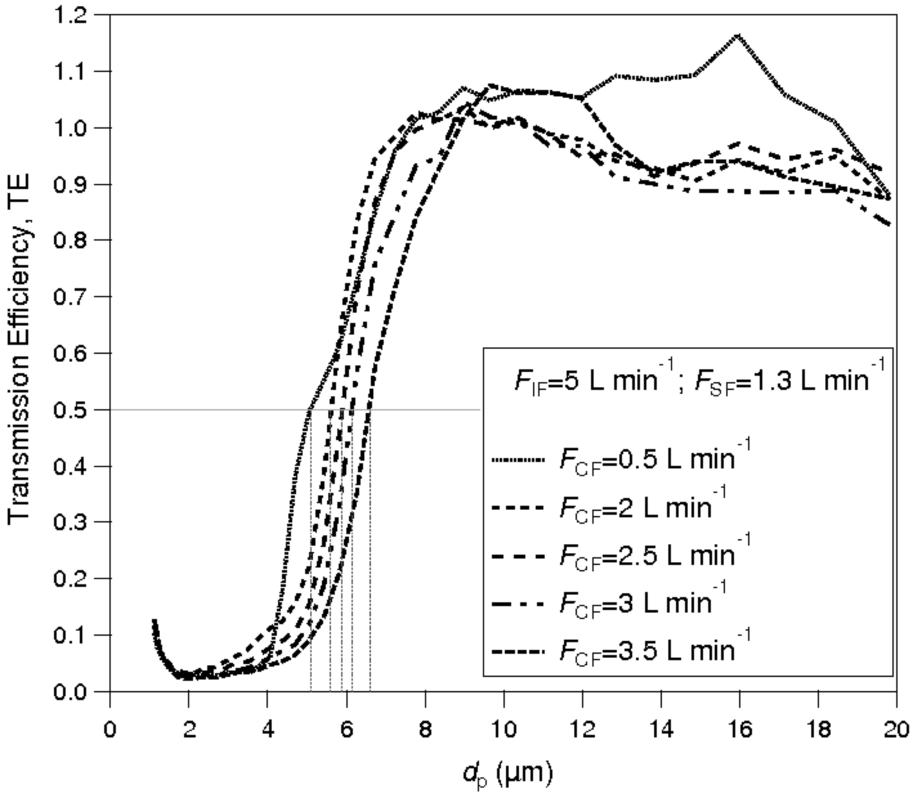

Figure 4. Transmission efficiency of the IN-PCVI derived from the number size distributions shown in Fig. 3. Vertical lines indicate the variation of $D_{p50\,\%}$ as a function of the counterflow.

AMTD
7, 10585–10617, 2014

Sampling of ambient ice nucleating particles

L. P. Schenk et al.

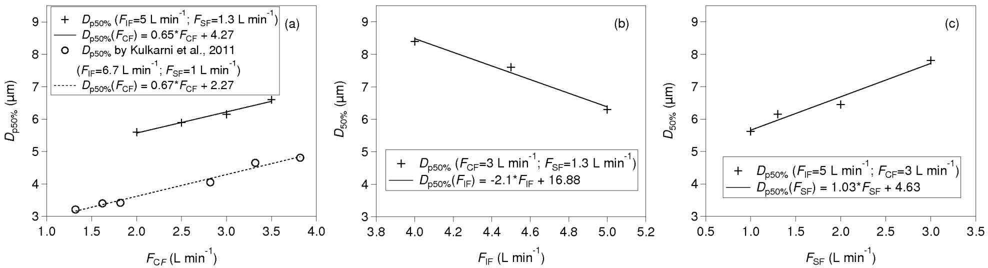

Figure 5. The IN-PCVI cut-off diameter, $D_{p50\,\%}$ for a changing **(a)** counterflow F_{CF}, **(b)** input flow F_{IF} and **(c)** sample flow F_{SF}. In **(a)** the variation of the $D_{p50\,\%}$ with F_{CF} as characterized by Kulkarni et al. (2011) is plotted as circles with a dashed regression line.

AMTD
7, 10585–10617, 2014

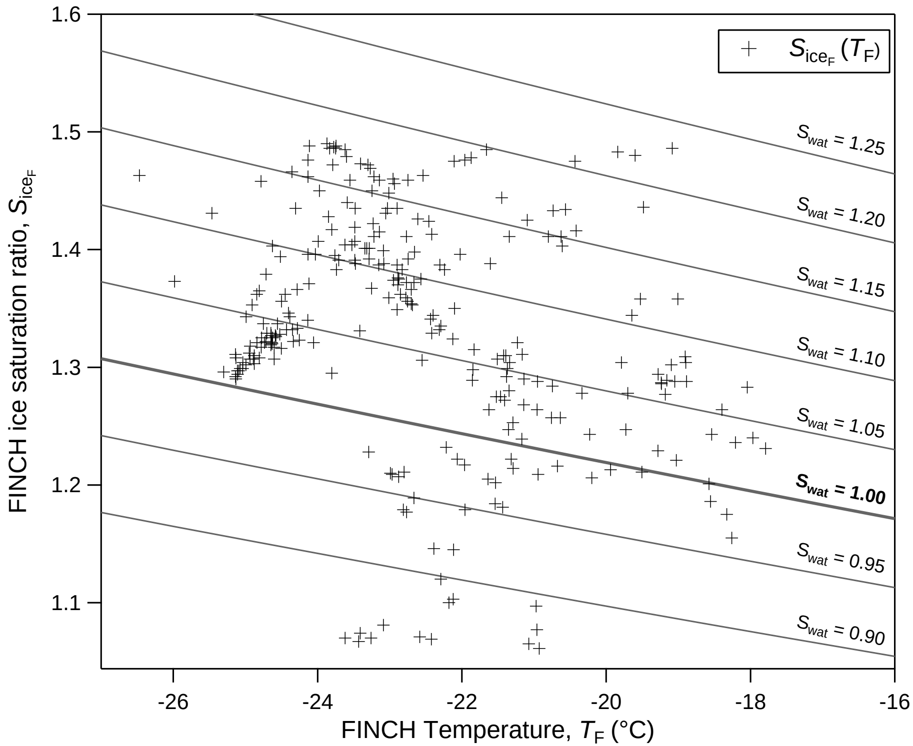

Figure 6. Ice activation conditions in FINCH cover a range of combinations of temperatures (T_F) and ice saturation ratios (S_{ice_F}). The majority of measurements was conducted at conditions supersaturated with respect to water (lines of constant S_{wat_F} are plotted in grey (0.05 steps)).

AMTD
7, 10585–10617, 2014

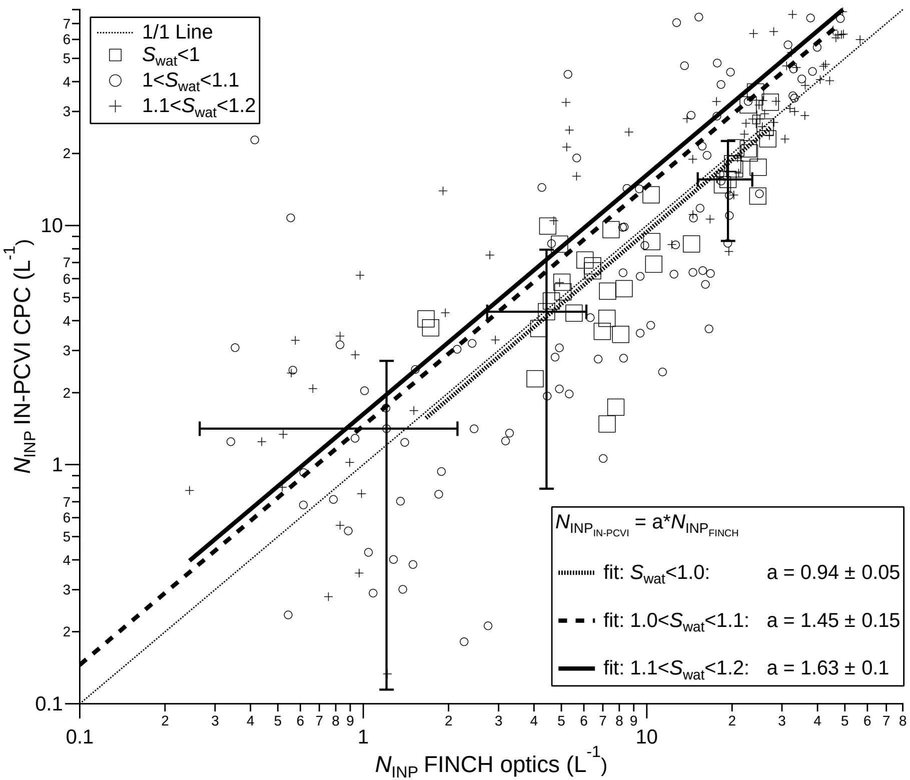

Figure 7. Scatter plot of the INP 10 min averaged number concentrations measured by the FINCH optics and the CPC of the IN-PCVI system, respectively. The concentrations are subdivided into three different water saturation ranges: $S_{wat_F} < 1.0$ (squares), $1.0 < S_{wat_F} < 1.1$ (circles) and $1.1 < S_{wat_F} < 1.2$ (crosses). The power regression curves (exponent equal 1) for these three classes are plotted as lines: $S_{wat_F} < 1.0$ (dotted line), $1.0 < S_{wat_F} < 1.1$ (dashed line) and $1.1 < S_{wat_F} < 1.2$ (solid line). For every number concentration range an example of the standard deviation is indicated by error bars.

AMTD
7, 10585–10617, 2014

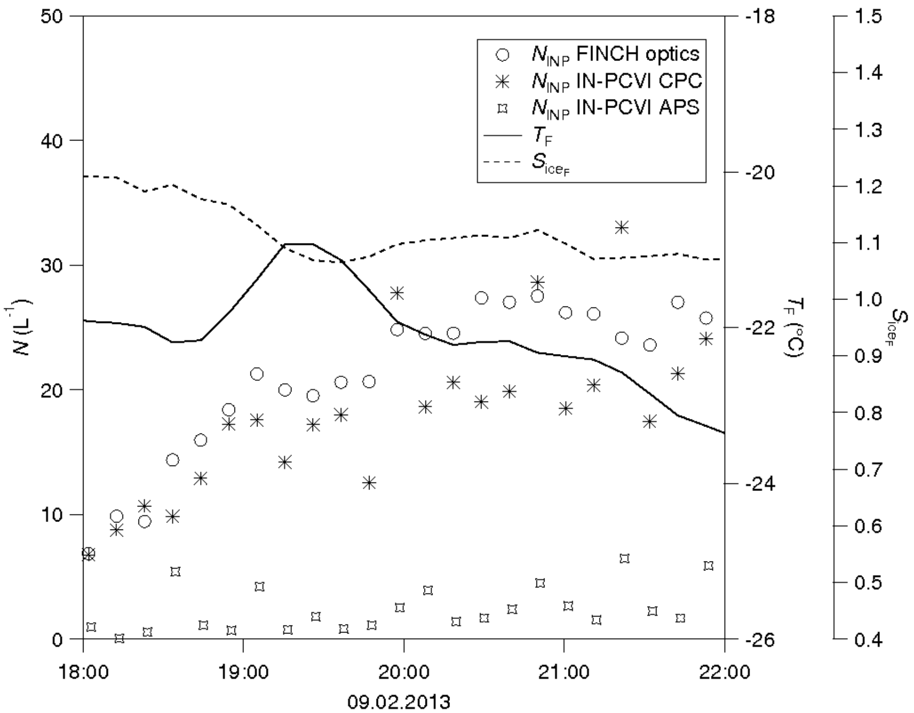

Figure 8. Time series of the INP number concentration (10 min averages) measured by the FINCH optics and by the IN-PCVI system (CPC and APS). The FINCH thermodynamic conditions are plotted as solid (temperature) and dashed (ice saturation) lines on the axes on the right hand side.

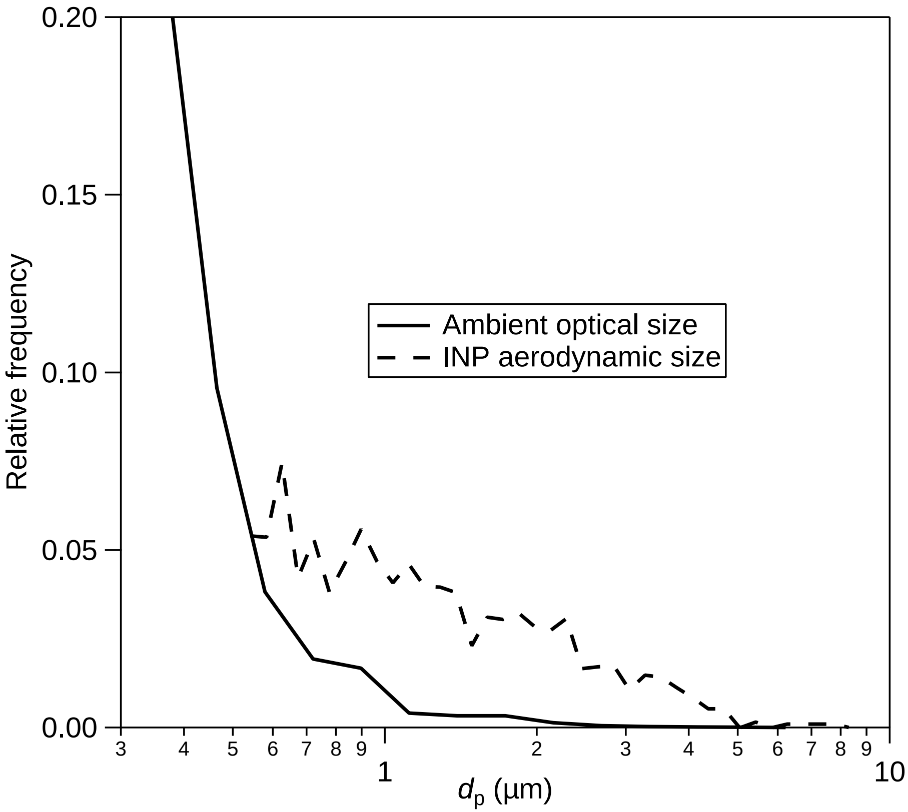

Figure 9. Relative frequency of the FINCH-INP sizes measured with the APS over the whole campaign period (dashed line) in comparison to the relative frequency of ambient aerosol particle sizes measured with an OPS (solid line).

AMTD
7, 10585–10617, 2014

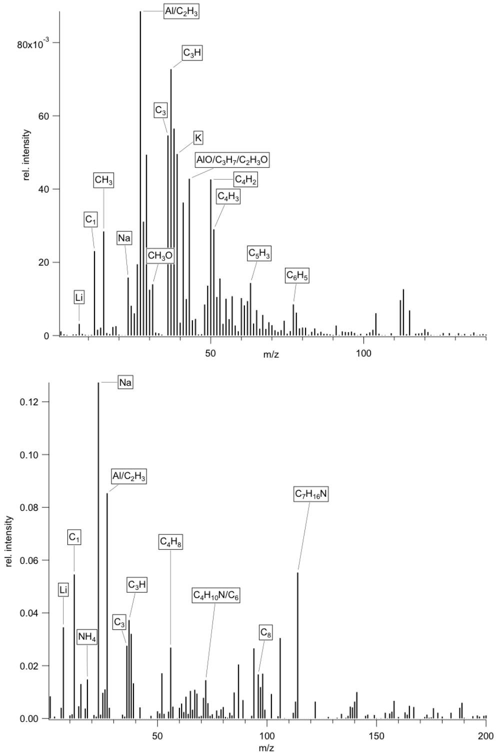

Figure 10. Examples for INP mass spectra measured online with the single particle mass spectrometer ALABAMA behind the FINCH + IN-PCVI. Both particle spectra are dominated by organic ions, but elements like Li and Al might also indicate that these particles may be mineral dust coated with organic matter.

AMTD
7, 10585–10617, 2014